

## Supporting Information

### Formation of Choline Salts and Dipolar Ions for CO<sub>2</sub> Reactive Eutectic Solvents

Ruth Dikki<sup>1</sup>, Eda Cagli<sup>1</sup>, Drace Penley<sup>1</sup>, Metin Karayilan<sup>2</sup>, Burcu Gurkan<sup>\*,1</sup>

<sup>1</sup> Department of Chemical and Biomolecular Engineering, Case Western Reserve University, Cleveland, OH

<sup>2</sup> Department of Chemistry, Case Western Reserve University, Cleveland, OH

\* Corresponding: beg23@case.edu

#### Table of Contents (30 pages)

Materials and Method descriptions

23 Figures (full NMR spectra enclosed)

2 Schemes

4 Tables

References

#### Materials

Imidazole (ImH) (99%, Thermo Scientific), 1,2,4-triazole (TrzH) (98%, Sigma-Aldrich), pyrrole-2-carbonitrile (CNpyrH) (99%, Alfa Aesar), phenol (PhOH) (98%, Sigma-Aldrich), and ethylene glycol (EG) (99.8%, Sigma-Aldrich) were used as received. Choline chloride salt ([Ch]<sup>+</sup>[Cl]<sup>-</sup>) (99%, Sigma-Aldrich) was dried for three days at 100 °C prior to use. Hydroxide-form anion exchange resin (A600-OH, Purolite) was washed with methanol before use. Other chemicals including silver nitrate (0.171N, Ricca), methanol (99.8%, HPLC grade, Fischer), and deuterated dimethyl sulfoxide (DMSO-d<sub>6</sub>, 99.9%), were used as received. The high purity CO<sub>2</sub> (99.995%) used for the CO<sub>2</sub> absorption experiment was obtained from Airgas.

#### Hydrogen Bond Acceptors and Eutectic Solvents Synthesis

A two-step anion exchange reaction procedure was followed as previously described by Lee *et al.*<sup>1</sup> Briefly, [Ch]<sup>+</sup>[Cl]<sup>-</sup> salt was converted into choline hydroxide [Ch]<sup>+</sup>[OH]<sup>-</sup> solution in methanol using an anion exchange resin, with complete conversion assessed using the silver nitrate test. About equimolar amounts of the anion precursors, listed in Table S1, was added to the solution and stirred at room temperature for 24 hours. The samples were then dried by rotary evaporation at 50 °C, and under vacuum at 50 °C for 2 days. The eutectic solvents were formed by mixing 1 to 2 molar ratios of the synthesized hydrogen bond acceptors (HBAs) with EG hydrogen bond donor

(HBD) at 40 °C before cooling to room temperature. The water content of the eutectic solvents formed were measured using a Karl Fischer titrator (Metrohm Coulometric KF 889D).

### **Hydrogen Bond Acceptors and Eutectic Solvents Characterization**

The chemical and structural analysis of the HBAs were performed with proton ( $^1\text{H}$ ) and carbon-13 ( $^{13}\text{C}$ ) Nuclear magnetic resonance (NMR) (Bruker 500 MHz) and attenuated total reflectance-Fourier transform infrared spectroscopy (ATR-FTIR) (Nicolet iS50 FTIR, Thermo Scientific). The thermal characterization of the synthesized HBAs, and their respective eutectic solvents with EG, was carried out with differential scanning calorimetry (DSC) (Mettler Toledo DSC3) and thermogravimetric analysis (TGA) (TGA500, TA instruments). From the TGA, the onset degradation temperatures ( $T_{\text{onset}}$ ) were determined by holding the samples isothermal for 15 minutes at 40 °C, before ramping up to 300 °C at 10 °C/min, and under 100 mL/min nitrogen flow.  $T_{\text{onset}}$  of the HBAs and the eutectic solvents were taken as the temperature where 5% mass loss had occurred. DSC characterization was done at a temperature range of -150 °C to 40 °C, with the rate of sample heating and cooling set to 10 °C/min and -10 °C/min, respectively. The samples were initially heated from 25 °C to 40 °C and held isothermally for 10 mins before cooling down to -150 °C under  $\text{N}_2$  atmosphere and reheating, with the final heating scan reported.

### **$\text{CO}_2$ Absorption and Thermal Swing Desorption**

About 0.5 g of the eutectic solvents was placed in a scintillator vial and saturated with  $\text{CO}_2$  at  $25 \pm 1$  °C, under 1 bar of  $\text{CO}_2$ . NMR techniques including  $^1\text{H}$  and quantitative carbon-13 ( $q\text{-}^{13}\text{C}$ ) NMR were combined with heteronuclear single quantum coherence (HSQC), heteronuclear multiple bond correlation (HMBC), and distortionless enhancement by polarization transfer (DEPT) analysis techniques to determine the reaction pathways and  $\text{CO}_2$  binding sites. 0.1 M of chromium (III) acetylacetonate solution in DMSO- $d_6$  was used for the  $q\text{-}^{13}\text{C}$  NMR analysis. The thermal swing desorption of  $\text{CO}_2$  was done by purging  $\text{N}_2$  through the  $\text{CO}_2$  saturated eutectic solvents at 70 °C (for the  $\text{Ch}^\pm\text{ImH}$  based eutectic solvents), and 50 °C (for the  $[\text{Ch}]^+[\text{Trz}]^-$ ,  $[\text{Ch}]^+[\text{CNPy}]^-$ , and  $\text{Ch}^\pm\text{PhOH}$  based eutectic solvents). The reaction cells were weighed at 5 mins intervals on an analytical balance ( $\pm 0.1$  mg) and when the mass returned to initial experiments were stopped.

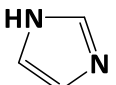
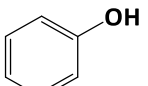
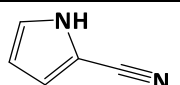
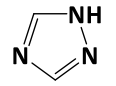
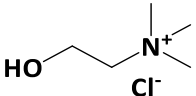
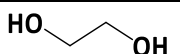
### **Breakthrough Experiments**

The  $\text{CO}_2$  breakthrough measurements were performed similarly as reported by Lee *et al.*,<sup>2</sup> where about 2.6 - 2.8 mL of the eutectic solvent was spread on the bottom of a 125 mL flat-bottom Pyrex flask. 200 mL/min feed gas (5000 ppm  $\text{CO}_2$  in  $\text{N}_2$ ) was allowed to pass through the sample, while the effluent  $\text{CO}_2$  concentration was monitored with a  $\text{CO}_2$  analyzer (SBA-5, PPSystems Inc.). The feed conditions are similar to the  $\text{CO}_2$  levels in the International Space Station and cabin air; representing a model gas feed for air revitalization applications. The microwave-assisted desorption was performed at 50 °C by auto adjusting the microwave power (between 0 - 10 W at 2.45 GHz), while the thermal desorption was done at 50 °C fixed temperature in an oil bath.

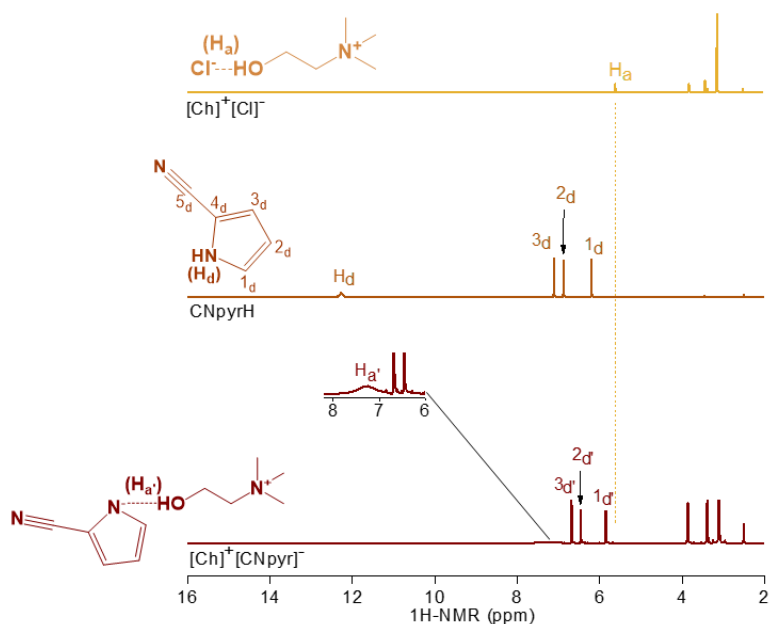
## Computational Methods

Calculations at the level of density function theory (DFT) was performed to understand the energetics involved in the formation of  $[\text{Ch}]^+$  and  $\text{Ch}^\pm$  based compounds. Quantum mechanics calculations were carried out in the Gaussian16 program,<sup>3</sup> using the three-parameter Becke model and Lee-Yang-Par modification (B3LYP) functional<sup>4</sup> for exchange and correlation, coupled with 6-311G++(d,p) basis set.<sup>5</sup> The simulation box consisted of a pair of  $[\text{Ch}]^+$  cation with a specific anion initially oriented to share the -OH proton on  $[\text{Ch}]^+$ . The energetics calculations were performed for both the  $[\text{Ch}]^+$  salts and the  $\text{Ch}^\pm$  based sorbents, with values compared to determine the potentially favorable product. It should be noted that to prevent the immediate transfer of the protons back to  $[\text{Ch}]^+$  during optimization, the  $\text{O}^-$  group on  $\text{Ch}^\pm$  was positioned to face the direction opposite to the proton. Uncertainty of the calculated energies was performed using Counterpoise, in which the individual molecules were separated in their own group to produce a Basis Set Superposition Error of 0.0014 Hartree. To mimic solvation by ethylene glycol, the optimized geometries of the choline salt and choline di-ion systems were used, and then two EG molecules were added and the structures were reoptimized.

**Table S1.** Molecular structures of the hydrogen bond donor (HBD) and hydrogen bond acceptors (HBAs) used for the synthesis of the eutectic solvents ( $\text{p}K_a$  values in bracket are in water).

Name	$\text{p}K_a$ in DMSO	Structure
<b>HBA or HBA precursor</b>		
Imidazole (ImH)	18.60 <sup>6</sup> (14.52) <sup>7</sup>	
Phenol (PhOH)	18.00 <sup>8</sup> (10.00) <sup>6</sup>	
Pyrrole-2-carbonitrile (CNpyrH)		
1,2,4-Triazole (TrzH)	13.90 <sup>6</sup> (9.97) <sup>7</sup>	
Choline chloride ( $[\text{Ch}]^+[\text{Cl}]^-$ )	(13.90) <sup>9</sup>	
<b>HBD</b>		
Ethylene glycol (EG)		

(a)



(b)

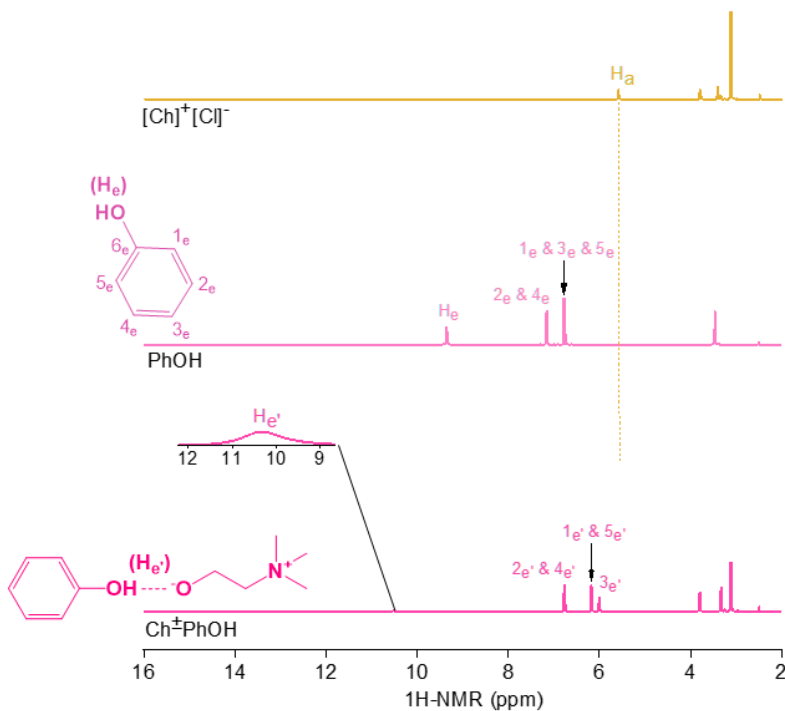
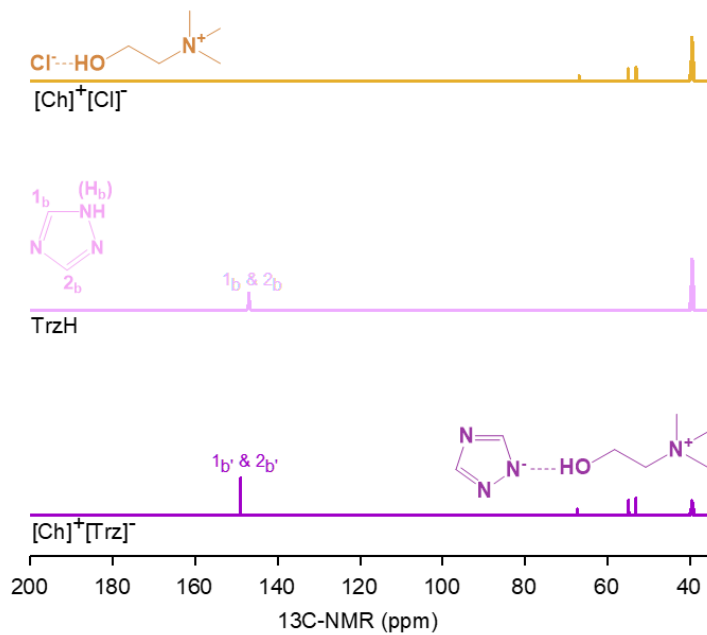


**Figure S1.** <sup>1</sup>H-NMR spectra of (a) [Ch]<sup>+</sup>[CNpyr]<sup>-</sup> and (b) Ch<sup>±</sup>PhOH HBAs and their precursors in DMSO-d<sub>6</sub>. The smaller inset peaks (H<sub>a'</sub> and H<sub>e'</sub>) integrate to approximately 1. The dotted lines represent intermolecular proton sharing and hydrogen bonding interactions.

(a)



(b)

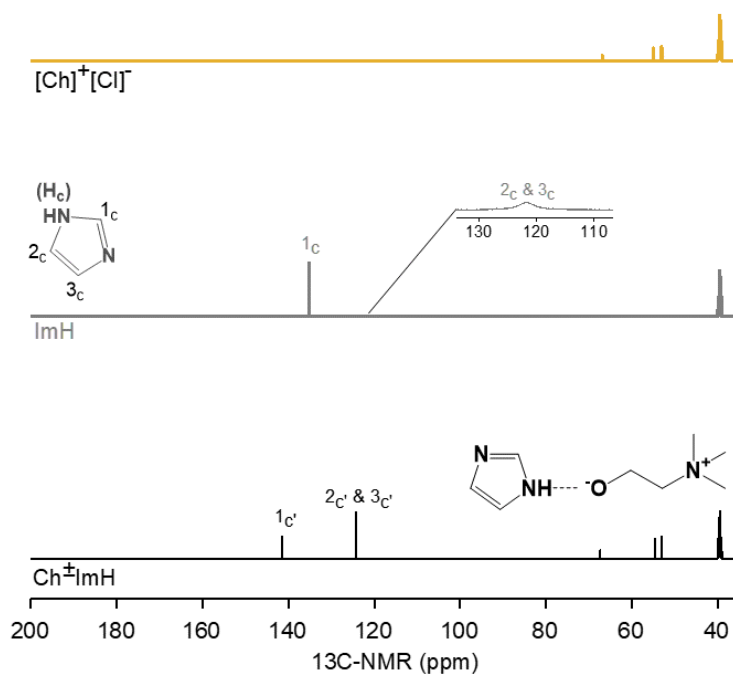
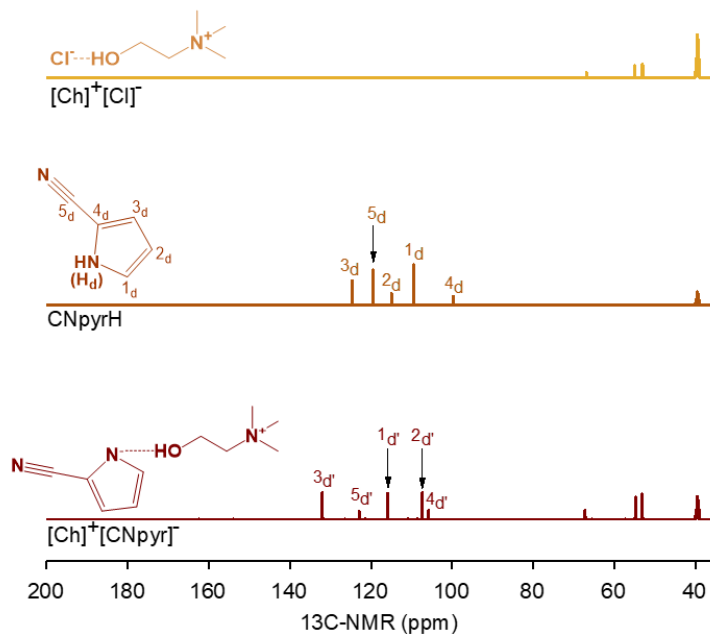


**Figure S2.**  $^{13}\text{C}$ -NMR of (a)  $[\text{Ch}]^+[\text{Trz}]^-$  and (b)  $\text{Ch}^\pm\text{ImH}$  HBAs and their precursors in DMSO- $d_6$ .

(a)



(b)

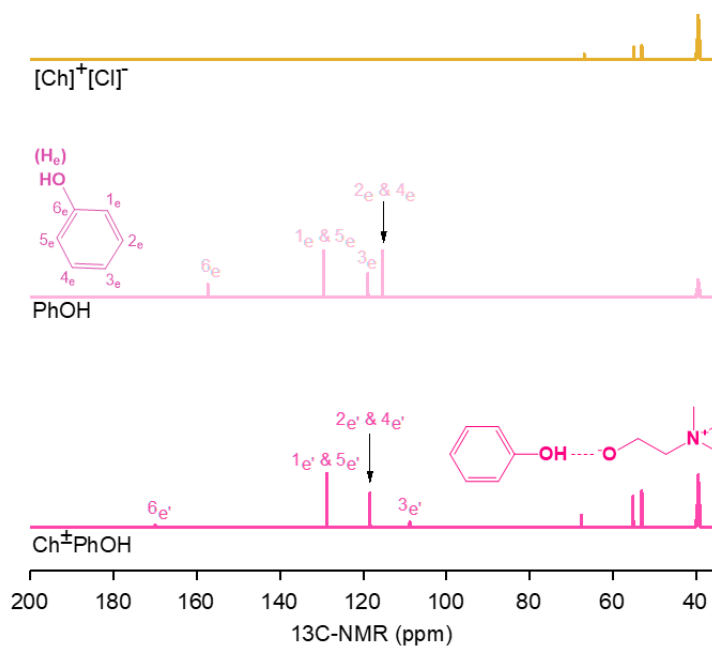


**Figure S3.**  $^{13}\text{C}$ -NMR of (a)  $[\text{Ch}]^+[\text{CNpyr}]^-$  and (b)  $\text{Ch}^\pm\text{PhOH}$  HBAs and their precursors in DMSO- $d_6$ .

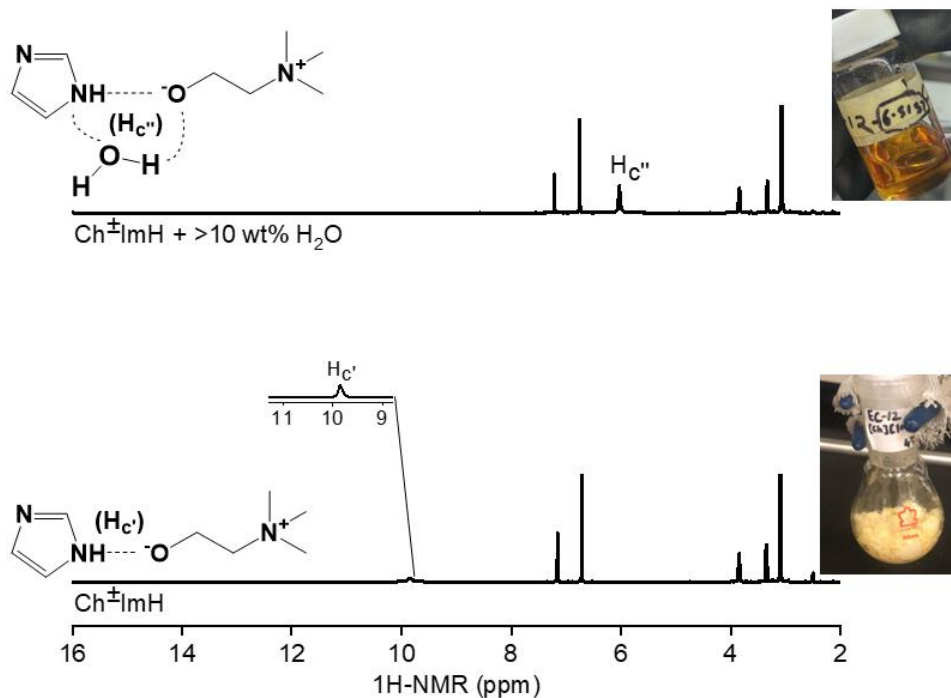


**Figure S4.** H<sub>c'</sub> chemical shift from 9.85 to 6.03 ppm with Ch<sup>±</sup>ImH moisture content of about 0.2% and >10%, respectively (the dotted lines represent intermolecular proton sharing and hydrogen bonding interactions). The water content reported for the solid Ch<sup>±</sup>ImH (i.e., 0.2%) is the moisture content of the eutectic solvents formed with EG. Peak H<sub>b'</sub> integrated to 1.10, while peak H<sub>c''</sub> integrated to 3.80, indicating the presence of water protons. This control experiment demonstrates the importance of measuring and reporting water content in CO<sub>2</sub> chemisorbing eutectic solvents as the presence of water not only influences the physical properties but also CO<sub>2</sub> binding mechanism and NMR interpretations.

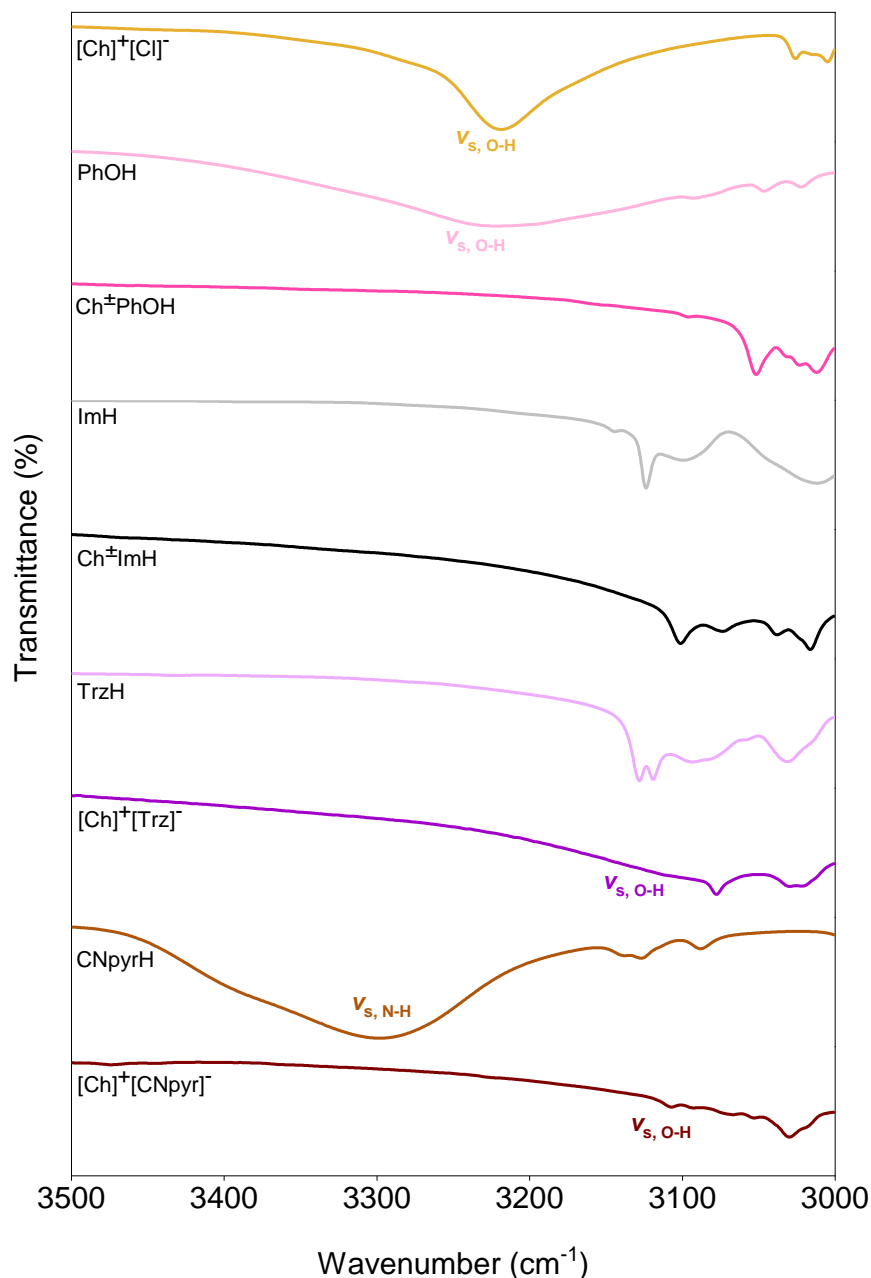


**Figure S5.** FTIR spectra showing N-H ( $\nu_{s, N-H}$ ) and O-H ( $\nu_{s, O-H}$ ) stretching vibrations in  $\text{Ch}^{\pm}\text{PhOH}$ ,  $\text{Ch}^{\pm}\text{ImH}$ ,  $[\text{Ch}]^+[\text{Trz}]^-$ , and  $[\text{Ch}]^+[\text{CNpyr}]^-$ , along with those observed in phenol (PhOH), imidazole (ImH), 1,2,4-triazole (TrzH), pyrrole-2-carbonitrile (CNpyrH), and  $[\text{Ch}]^+[\text{Cl}]^-$ . While the -OH vibration is seen in both  $[\text{Ch}]^+[\text{Cl}]^-$  and PhOH around the same region, no -OH stretching vibration is observed in  $\text{Ch}^{\pm}\text{PhOH}$  due to the strong hydrogen bonding interactions between choline and phenol hydroxyl groups. Suppression and even disappearance of IR vibrations related to -OH and -NH moieties is common for solvents with high degree of hydrogen bonding. One example is by Ryu *et al.*<sup>10</sup> where they reported the disappearance of free -NH peaks in mixtures with significant hydrogen bonding.



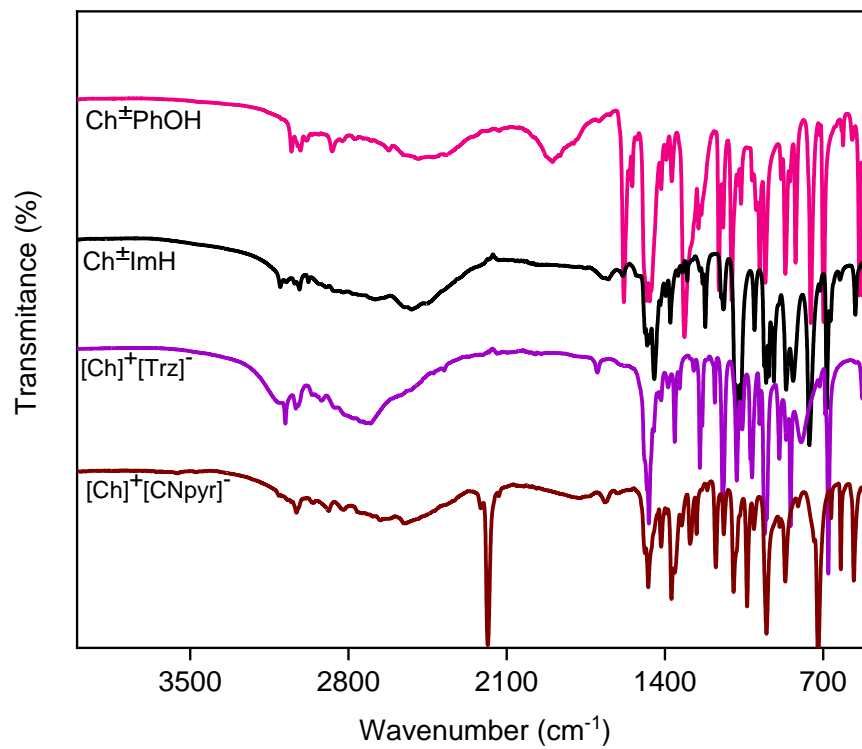


**Figure S6.** Full FTIR spectra of Ch<sup>±</sup>PhOH, Ch<sup>±</sup>ImH, [Ch]<sup>+</sup>[Trz]<sup>-</sup>, and [Ch]<sup>+</sup>[CNpyr]<sup>-</sup>.

**Table S2.** DFT energetics of the system with  $[\text{Ch}]^+$  ion and  $\text{Ch}^\pm$  dipolar ion.

System	E (Hartrees)	$[\text{Ch}]^+[\text{Anion}]^- - \text{Ch}^\pm \text{AnionH}$ (Hartrees)
$[\text{Ch}]^+[\text{Im}]^-$	-554.645	+0.006
$\text{Ch}^\pm \text{ImH}$	-554.651	
$[\text{Ch}]^+[\text{PhO}]^-$	-635.935	-0.004
$\text{Ch}^\pm \text{PhOH}$	-635.931	
$[\text{Ch}]^+[\text{CNpyr}]^-$	-630.878	-0.026
$\text{Ch}^\pm \text{CNpyrH}$	-630.852	
$[\text{Ch}]^+[\text{Trz}]^-$	-570.697	-0.027
$\text{Ch}^\pm \text{TrzH}$	-570.670	

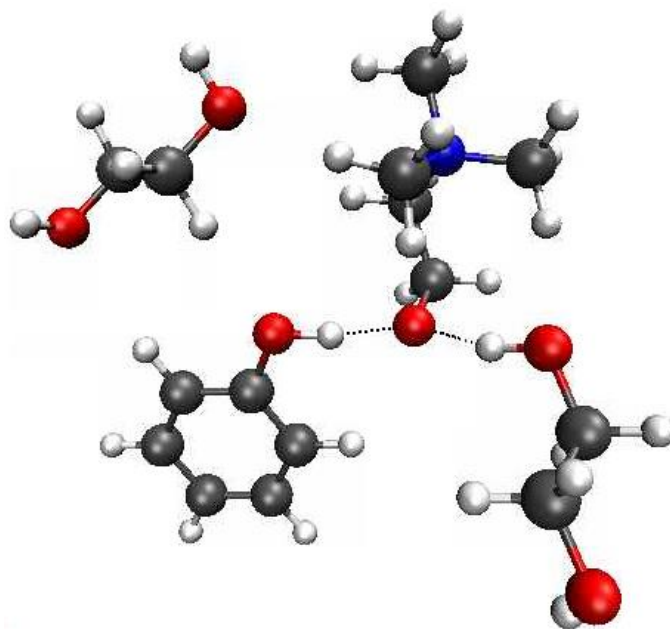


**Figure S7.** Optimized structure of  $\text{Ch}^\pm \text{PhOH}$  with 2 ethylene glycol molecules from Gaussian. It should be noted that whether the initial simulations included  $[\text{Ch}][\text{PhO}]$  or  $\text{Ch}^\pm \text{PhOH}$ , the structure was the same. Hydrogen bonds shown as black dashed lines. Color code: red (oxygen), grey (carbon), white (hydrogen), and blue (nitrogen).

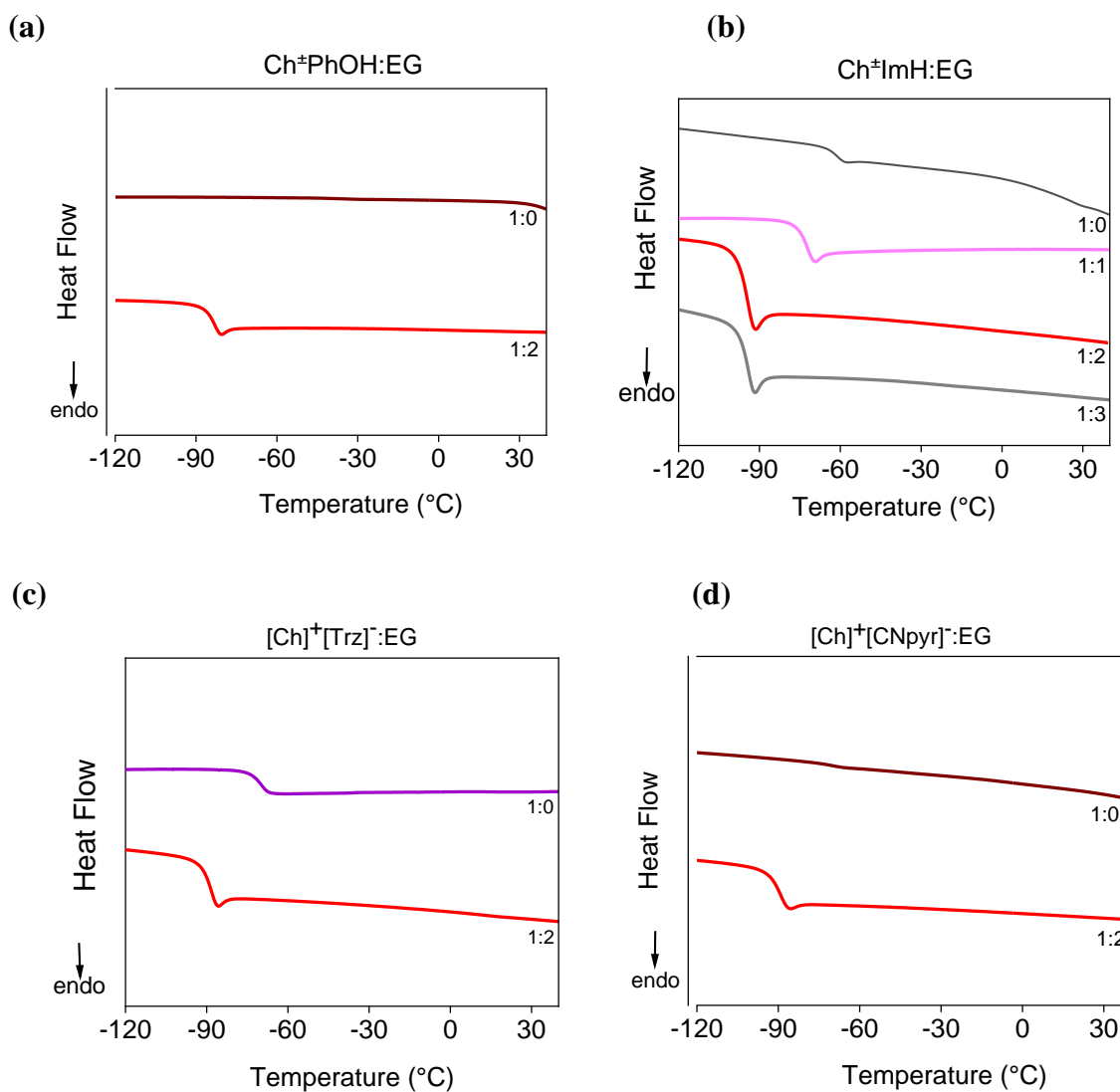


**Figure S8.** DSC thermograms of (a) Ch<sup>±</sup>PhOH, (b) Ch<sup>±</sup>ImH, (c) [Ch]<sup>+</sup>[Trz]<sup>-</sup>, and (d) [Ch]<sup>+</sup>[CNpyr]<sup>-</sup> HBAs and their EG based eutectic solvents. It should be noted that EG melting point is -11.5 °C.<sup>1</sup>

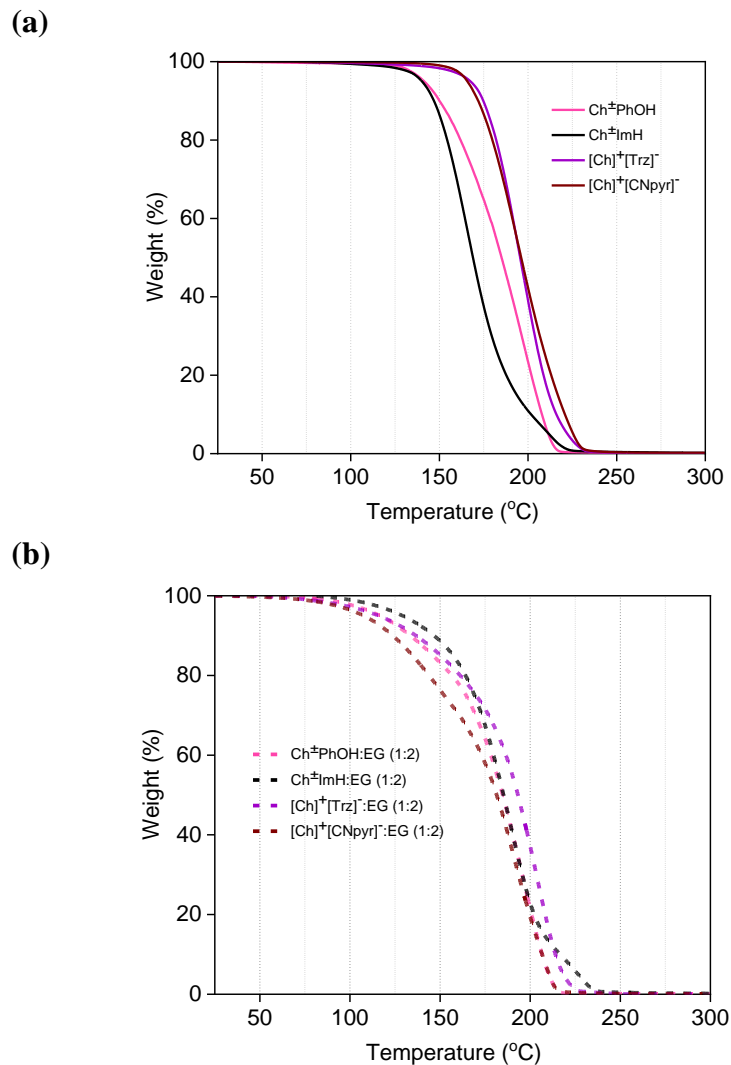


**Figure S9.** TGA curves of (a)  $\text{Ch}^\pm\text{PhOH}$ ,  $\text{Ch}^\pm\text{ImH}$ ,  $[\text{Ch}]^+[\text{Trz}]^-$ , and  $[\text{Ch}]^+[\text{CNpyr}]^-$  HBAs, with their (b) EG based eutectic solvents.

**Table S3.** Onset degradation temperatures of the HBAs and their corresponding eutectic solvents.

HBA		HBA:EG (1:2)
	$T_{\text{onset}}$ ( $^\circ\text{C}$ )	$T_{\text{onset}}$ ( $^\circ\text{C}$ )
$\text{Ch}^\pm\text{PhOH}$	141	116
$\text{Ch}^\pm\text{ImH}$	140	129
$[\text{Ch}]^+[\text{Trz}]^-$	165	107
$[\text{Ch}]^+[\text{CNpyr}]^-$	167	115

Note\*:  $T_{\text{onset}}$  represents the onset degradation temperature where 5% mass loss occurred.

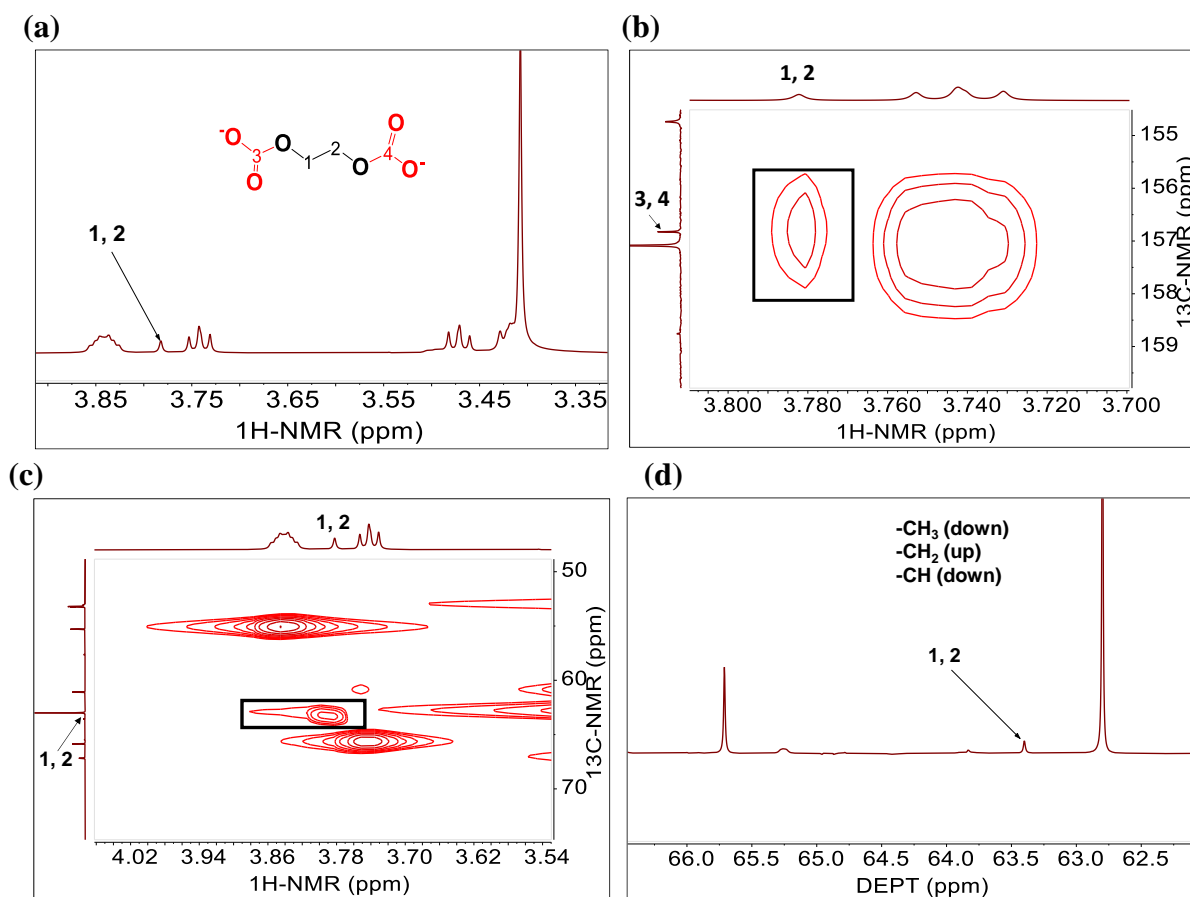


**Figure S10.** Product E in the  $\text{CO}_2$  saturated  $\text{Ch}^\pm\text{ImH}$  and EG eutectic solvent. (a) The absence of protons 1 and 2 peak splitting in the  $^1\text{H-NMR}$  supports the formation of a symmetrical dianion with identical protons. (b) HMBC NMR shows chemisorbed  $\text{CO}_2$  carbons (3 and 4) interacting with protons 1 and 2, therefore confirming the existence of a covalent bond between these atoms. (c) HSQC NMR shows the interactions of protons 1 and 2 with carbons 1 and 2, respectively, and (d) DEPT NMR shows the presence of  $\text{CH}_2$  carbons (1 and 2). Additionally,  $^1\text{H}$  and  $q\text{-}^{13}\text{C}$  NMR showed that carbons 3 and 4 integrated up to 0.13 moles, carbons 1 and 2 integrated up to 0.13, and protons 1 and 2 integrated up to 0.26 moles. The dianion is proposed to form from simultaneous binding of  $\text{CO}_2$  to both sides of the EG molecule.

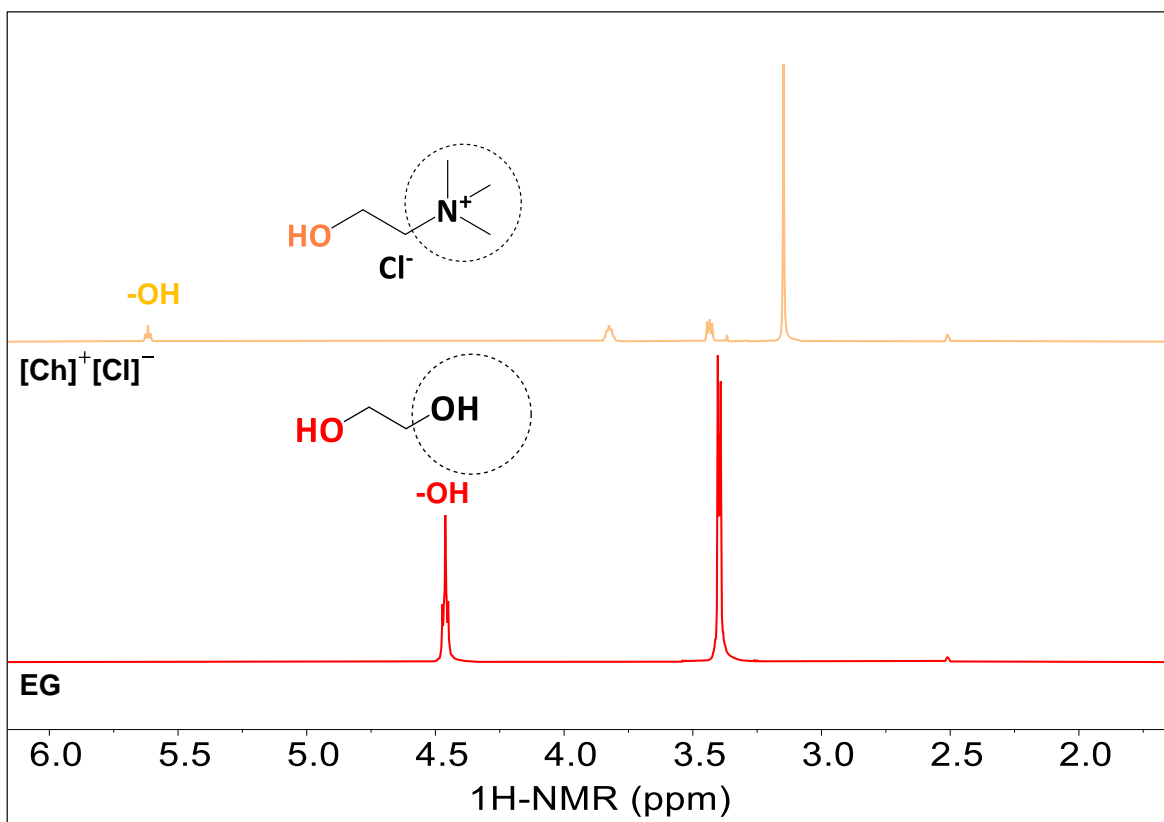


**Figure S11.** Comparison of -OH proton chemical shift in [Ch]<sup>+</sup>[Cl]<sup>-</sup> versus EG.

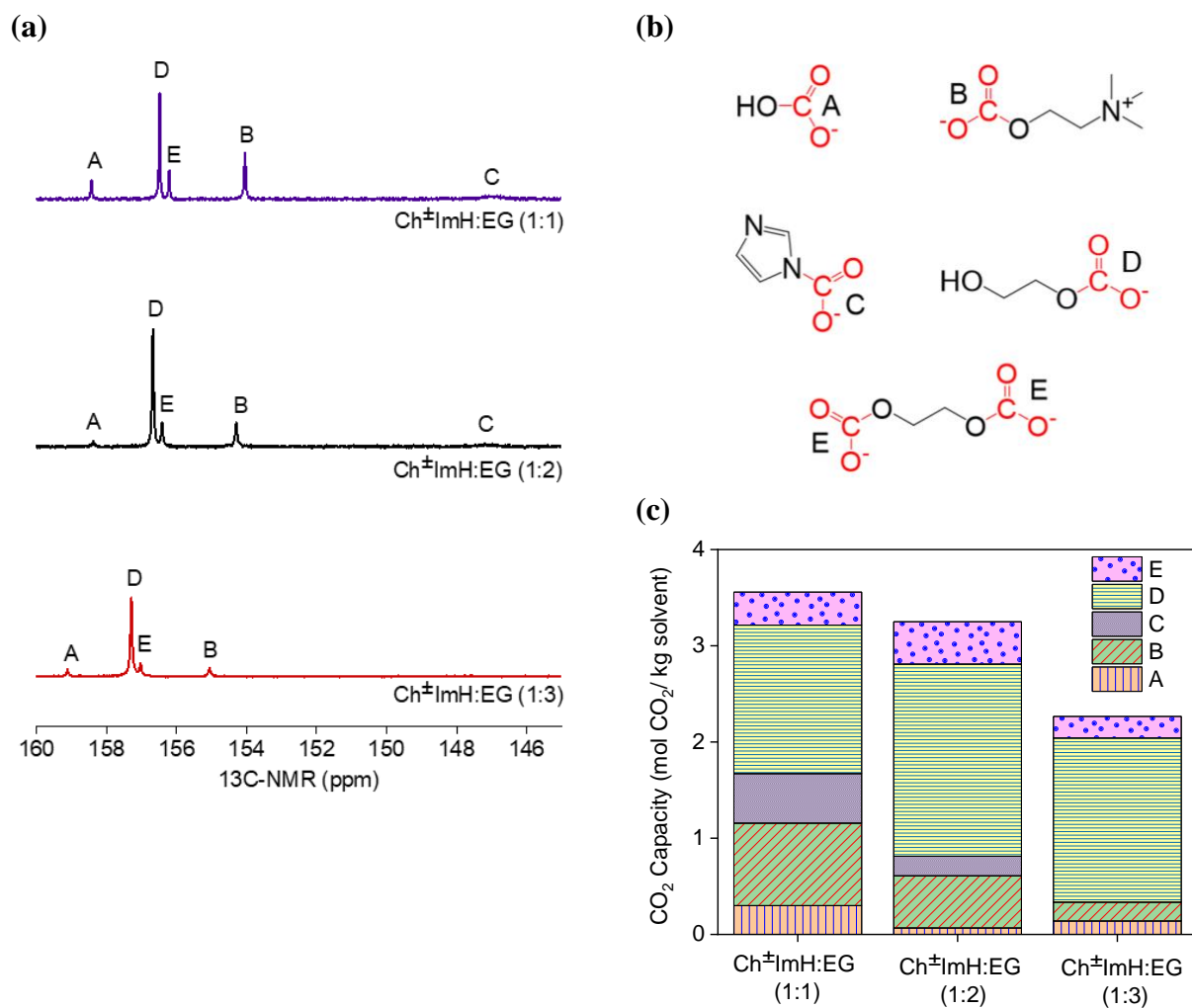


**Figure S12.** CO<sub>2</sub> saturated Ch<sup>±</sup>ImH:EG eutectic solvent showing (a) q-<sup>13</sup>C NMR peaks of the chemisorbed CO<sub>2</sub> (b) CO<sub>2</sub> binding sites determined from 1D- and 2D-NMR analysis, and (c) quantified CO<sub>2</sub> gravimetric capacities and product distributions obtained from q-<sup>13</sup>C NMR.

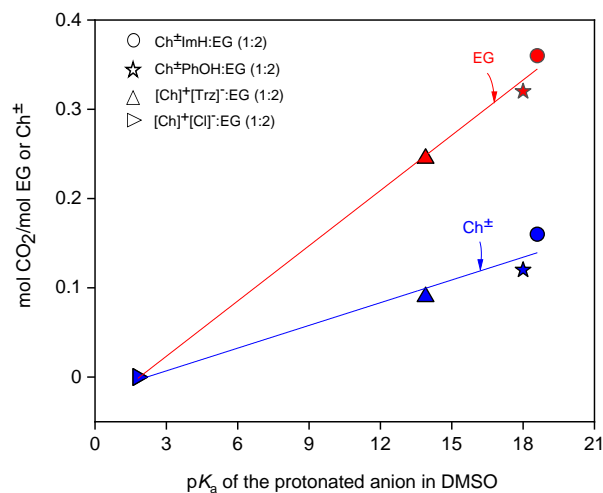
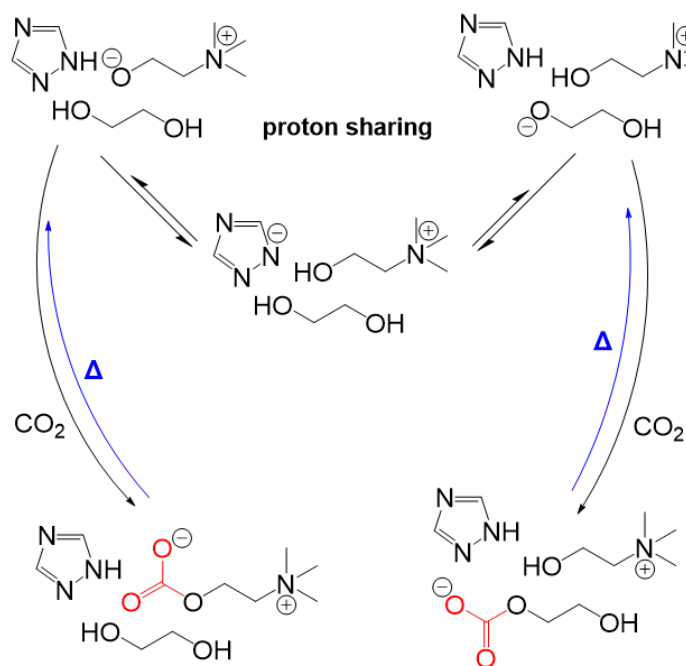


**Figure S13.** CO<sub>2</sub> binding to EG or Ch<sup>±</sup> as a function of the pK<sub>a</sub> of the protonated anion. CO<sub>2</sub> binding and desorption are related to one another and since the binding mechanism and strength changes according to the pK<sub>a</sub> of the precursor materials, the proton activity present in these solvents has a significant influence. While the hydrogen bonding typically results in induced electrostatics that weakens binding strength which can make it easier to desorb the CO<sub>2</sub> with reduced energy input (e.g., milder temperatures), a strong H-bonding network can also increase viscosity and present increased mass transfer limitations in a desorption column. Therefore, when designing eutectic solvents for chemisorption of CO<sub>2</sub>, factors such as viscosity, thermal stability and volatility besides pK<sub>a</sub> should be considered.





**Scheme S1.** Major CO<sub>2</sub> binding mechanisms in the [Ch]<sup>+</sup>[Trz]<sup>-</sup>:EG eutectic solvents.

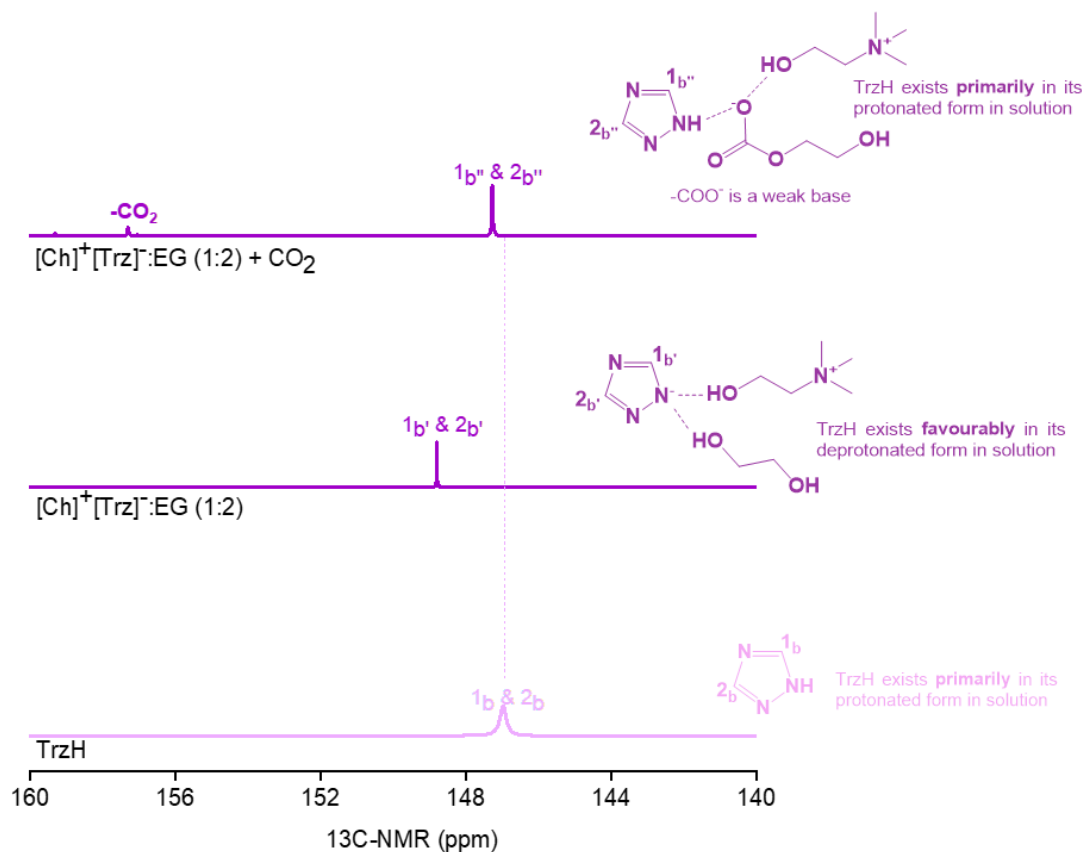
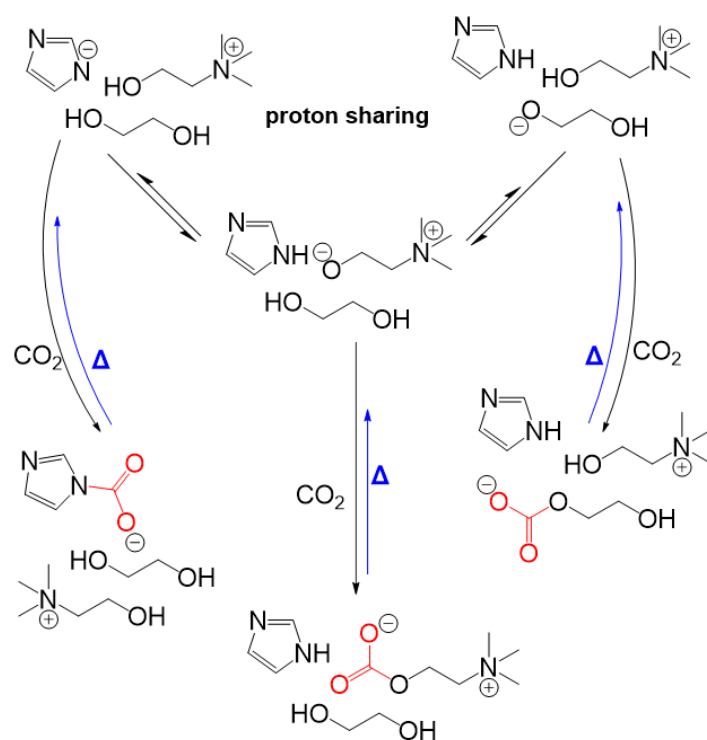


**Figure S14.**  $^{13}\text{C}$ -NMR spectra of TrzH anion precursor, with the neat and  $\text{CO}_2$  saturated  $[\text{Ch}]^+[\text{Trz}]^-$  based eutectic solvents. The upfield chemical shift of aromatic carbons  $1_b$  and  $2_b$  supports the presence of deprotonated TrzH in the neat solvent, which becomes predominantly protonated post  $\text{CO}_2$  chemisorption. Overlapping carbon peaks ( $1_{b'}$  and  $2_{b'}$  at 148.8 ppm) in the neat eutectic solvent experiences an upfield shift (147.3 ppm) after  $\text{CO}_2$  chemisorption, which is closer in proximity to carbons  $1_b$  and  $2_b$  in TrzH (147.0 ppm). In the  $\text{CO}_2$  saturated  $[\text{Ch}]^+[\text{Trz}]^-:\text{EG}$  (1:2),  $[\text{Trz}]^-$  exists primarily in its protonated form as TrzH.



**Scheme S2.** Major CO<sub>2</sub> binding mechanisms in the Ch<sup>+</sup>ImH:EG eutectic solvents.

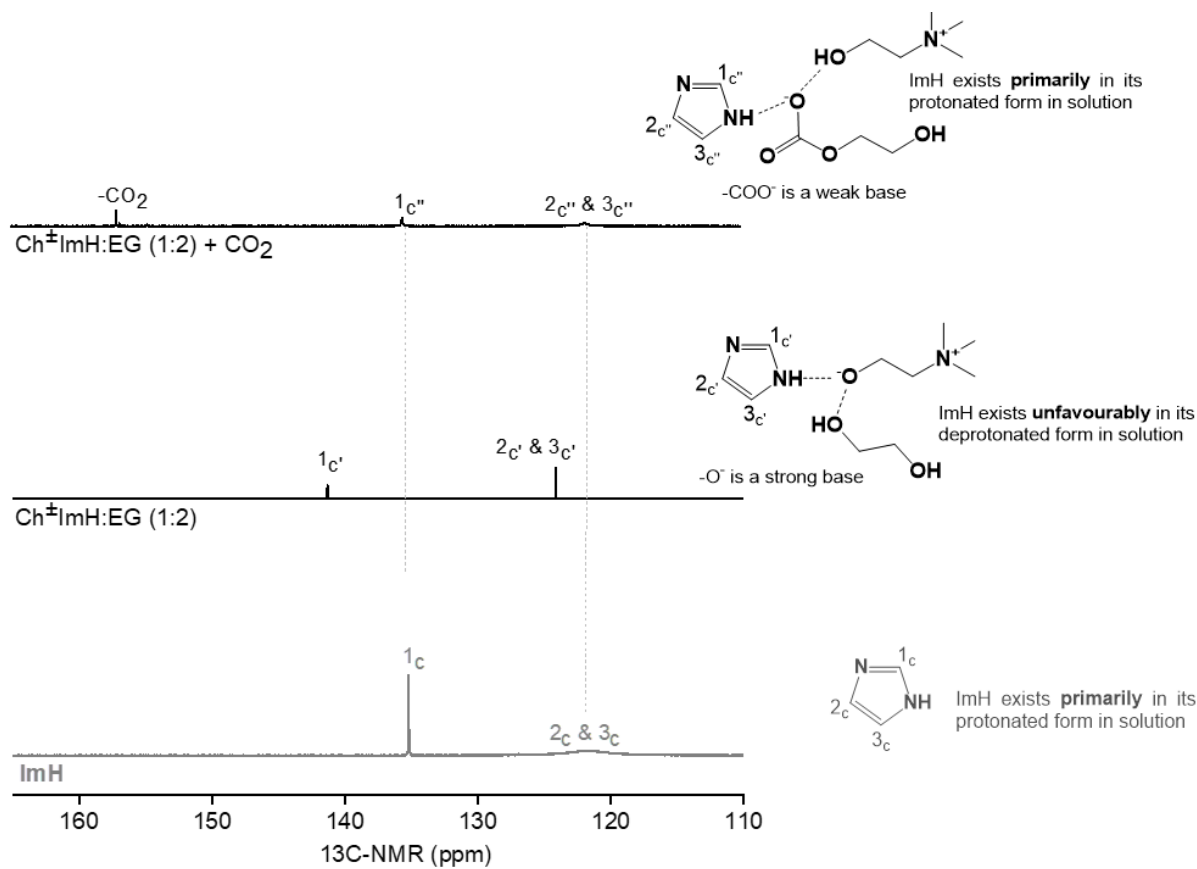


**Figure S15.**  $^{13}\text{C}$ -NMR of ImH anion precursor, with the neat and  $\text{CO}_2$  saturated  $\text{Ch}^\pm\text{ImH}$  based eutectic solvent. The chemical shifts of carbons  $1_c$ ,  $2_c$ , and  $3_c$  supports the presence of deprotonated ImH in the neat solvent, which becomes primarily protonated post  $\text{CO}_2$  chemisorption. This results from the high proton affinity of  $\text{Ch}^\pm$  which allows for the formation of  $[\text{Im}]^-$ .

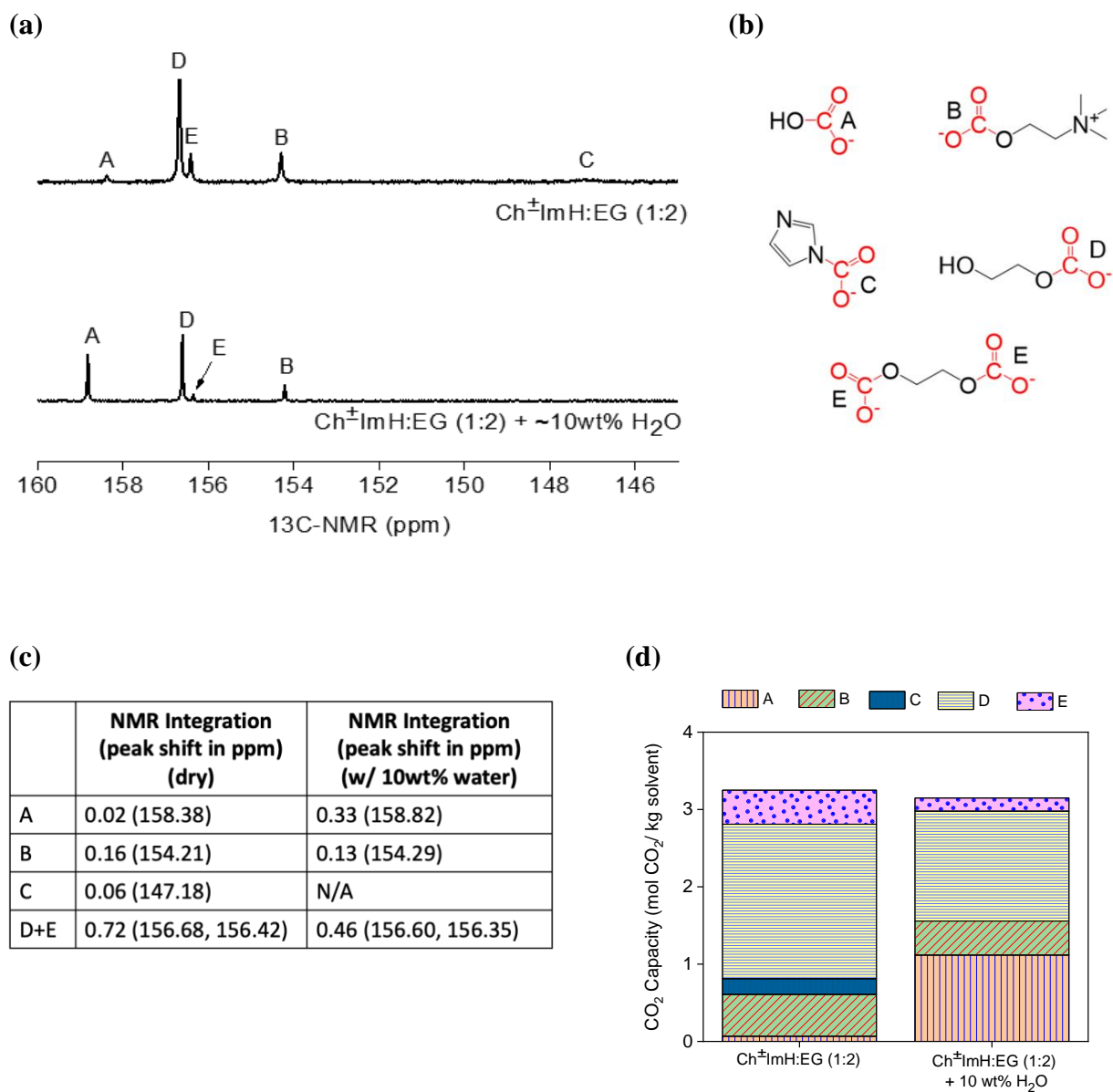


**Figure S16. Probing the bicarbonate (product A) formation with the inclusion of water:** CO<sub>2</sub> absorption with Ch<sup>±</sup>ImH:EG (1:2) eutectic solvent including 10 wt% water, compared to the dried sample (1500ppm water). (a) q-<sup>13</sup>C NMR; (b) identified absorption products; (c) peak integrations and shifts; and (d) quantified CO<sub>2</sub> gravimetric capacities with respect the binding sites. Intentional addition of water resulted in an increase in bicarbonate (product A) formation and a subsequent decrease in carbonate (products B, D, and E) and carbamate (product C) species, as evident from the peak intensities (i.e., bicarbonate peak, specie A, at ~160 ppm intensified with the addition of water in q-<sup>13</sup>C NMR in panel a).

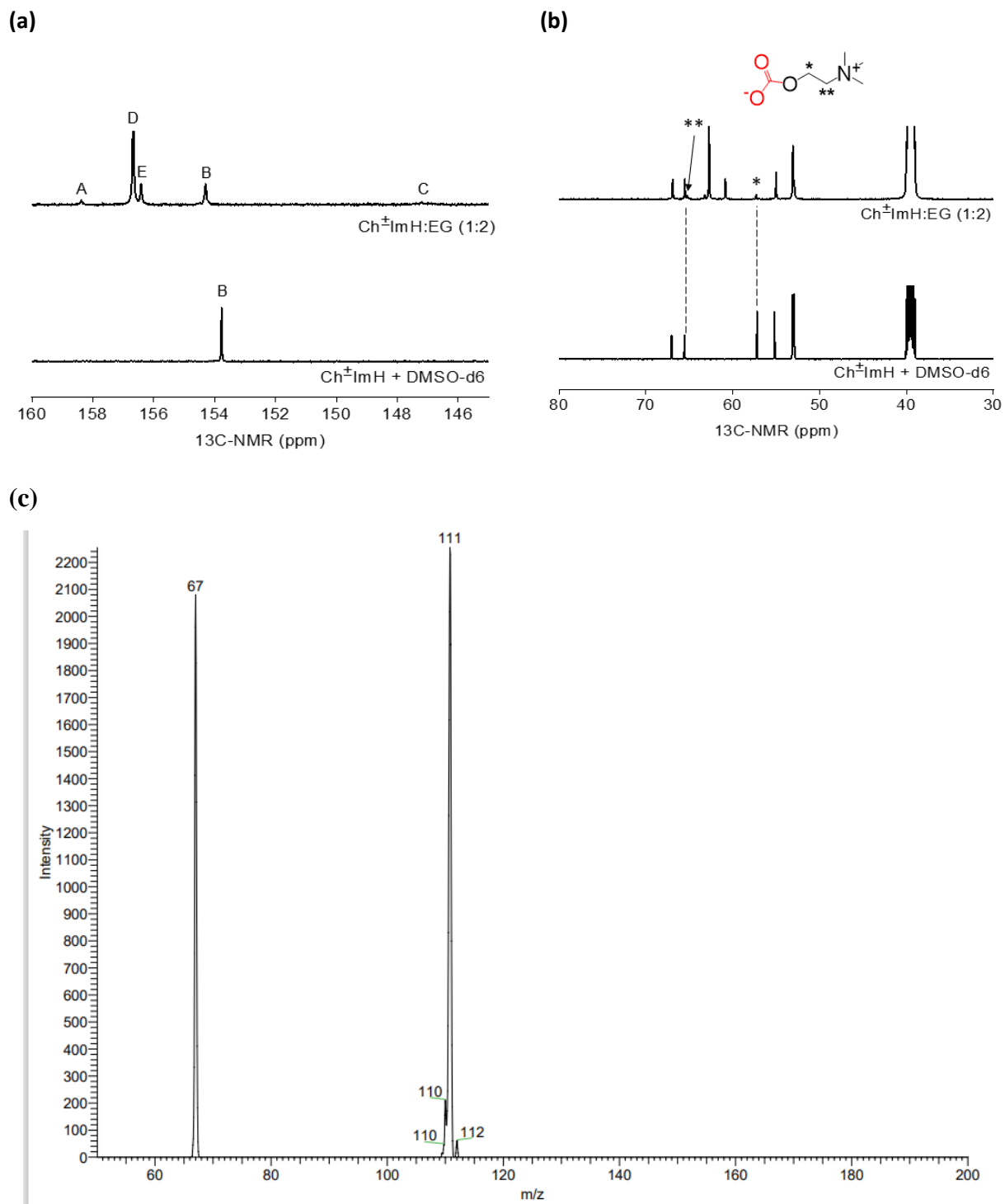


**Figure S17: Probing the  $[\text{Ch}]^+-\text{CO}_2^-$  (product B) and  $[\text{Im}]-\text{CO}_2^-$  (product C) formation:  $\text{CO}_2$  absorption of  $\text{Ch}^\pm\text{ImH}$  in  $\text{DMSO-d}_6$ , compared to  $\text{Ch}^\pm\text{ImH}:\text{EG}$  (1:2) eutectic solvent.** (a)  $q$ - $^{13}\text{C}$  NMR peaks of the chemisorbed  $\text{CO}_2$ . Product C is very low in concentration; therefore, it is further probed by ESI-MS. (b) Peak splitting of carbons \* and \*\* in 50-70 ppm region,

consistently observed in the presence and absence of EG, thus confirming peak B assignment for chemisorbed CO<sub>2</sub> to choline dipolar ion. (c) ESI-MS negative scan for the anions in CO<sub>2</sub> saturated Ch<sup>±</sup>ImH:EG (1:2), showing the breakdown of [Im]-COO<sup>-</sup> (molecular weight = 111.08 g/mol) to [Im]<sup>-</sup> (molecular weight = 67.07 g/mol). ESI-MS analyses were employed by electrospray ionization mass spectroscopy TSQ Quantum XLS Ultra. Samples with a concentration of about 100 μM in acetonitrile mixture were directly infused and scanned in the range of m/z 50–600.

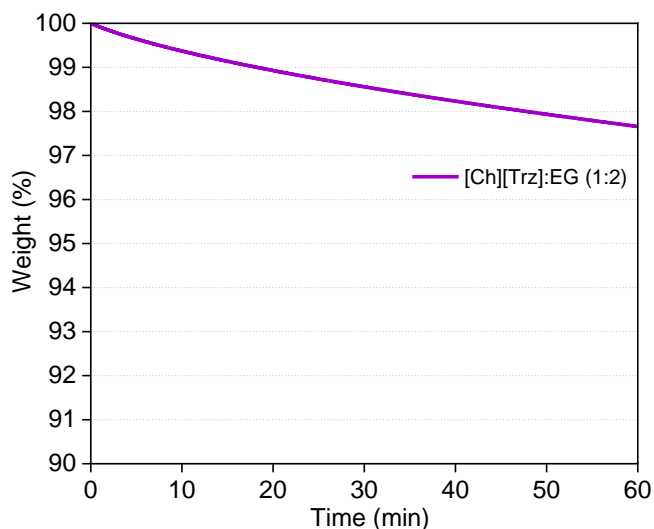


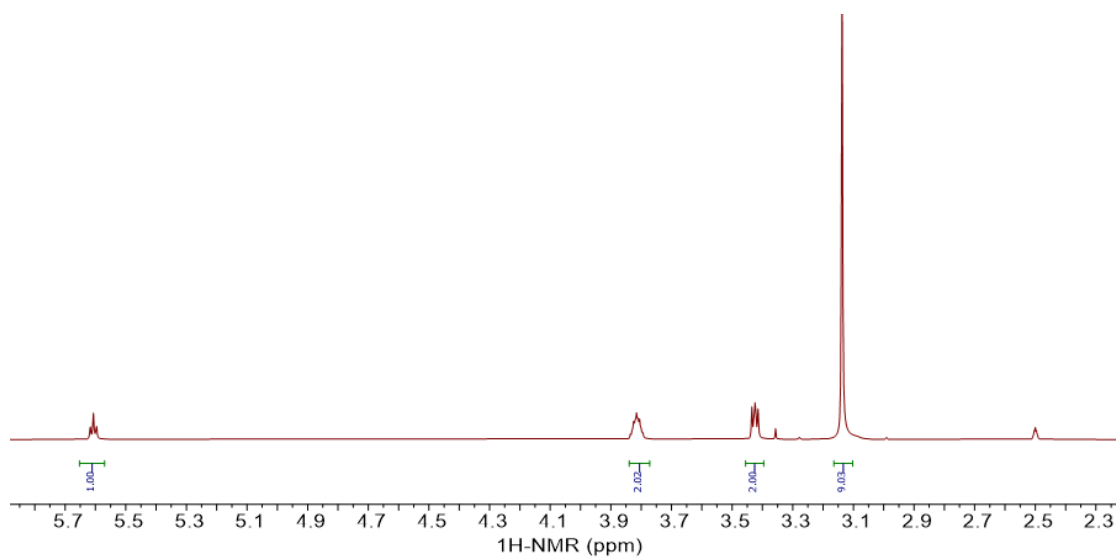
**Figure S18.** TGA isothermal curve of [Ch]<sup>+</sup>[Trz]<sup>-</sup>:EG (1:2) eutectic solvent at 50 °C.

**Table S4.** CO<sub>2</sub> capacities of different eutectic solvents at 1 bar CO<sub>2</sub>, and 25 °C. Refs.<sup>11,12</sup> do not report CO<sub>2</sub> capacities obtained from q-<sup>13</sup>C NMR integrations.

Solvent	Regeneration under N <sub>2</sub>	CO <sub>2</sub> Capacity (mol CO <sub>2</sub> /kg solvent)	Ref
[Ch] <sup>+</sup> [Cl] <sup>-</sup> :Glycerol:DBN (1:3:10)	60 °C	2.36	13
[Ch] <sup>+</sup> [Pro] <sup>-</sup> :EG (1:2)	50 °C	2.10	14
[Ch] <sup>+</sup> [Phe] <sup>-</sup> :EG (1:2)	-	0.45	14
[Ch] <sup>+</sup> [Gly] <sup>-</sup> :EG (1:2)	-	1.69	14
[Ch] <sup>+</sup> [βAla] <sup>-</sup> :EG (1:2)	-	1.83	14
[N <sub>2222</sub> ] <sup>+</sup> [3_Trz] <sup>-</sup> :EG (1:2)	60 °C	2.48	11
[N <sub>2222</sub> ] <sup>+</sup> [3_Trz] <sup>-</sup> :3_TrzH (1:2)	-	0.24	11
[N <sub>2222</sub> ] <sup>+</sup> [Trz] <sup>-</sup> :EG (1:2)	-	2.85	12
[N <sub>2222</sub> ] <sup>+</sup> [Im] <sup>-</sup> :EG (1:2)	-	2.96	12
[P <sub>2222</sub> ] <sup>+</sup> [Trz] <sup>-</sup> :EG (1:2)	70 °C	2.68	12
[P <sub>2222</sub> ] <sup>+</sup> [Im] <sup>-</sup> :EG (1:2)	-	2.69	12
[EMIM] <sup>+</sup> [CNpyr] <sup>-</sup> :EG (1:2)	40 °C	2.59	1
Ch <sup>±</sup> PhOH:EG (1:2)	50 °C	2.49	This study
Ch <sup>±</sup> ImH:EG (1:2)	70 °C	3.25	This study
[Ch] <sup>+</sup> [Trz] <sup>-</sup> :EG (1:2)	50 °C	2.36	This study
[Ch] <sup>+</sup> [CNpyr] <sup>-</sup> :EG (1:2)	50 °C	2.41	This study



(a)



(b)

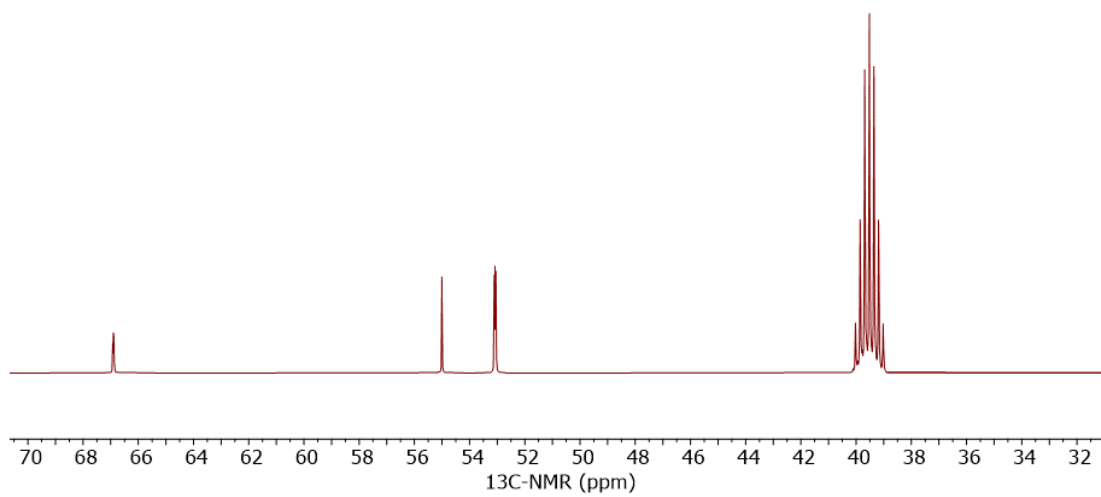
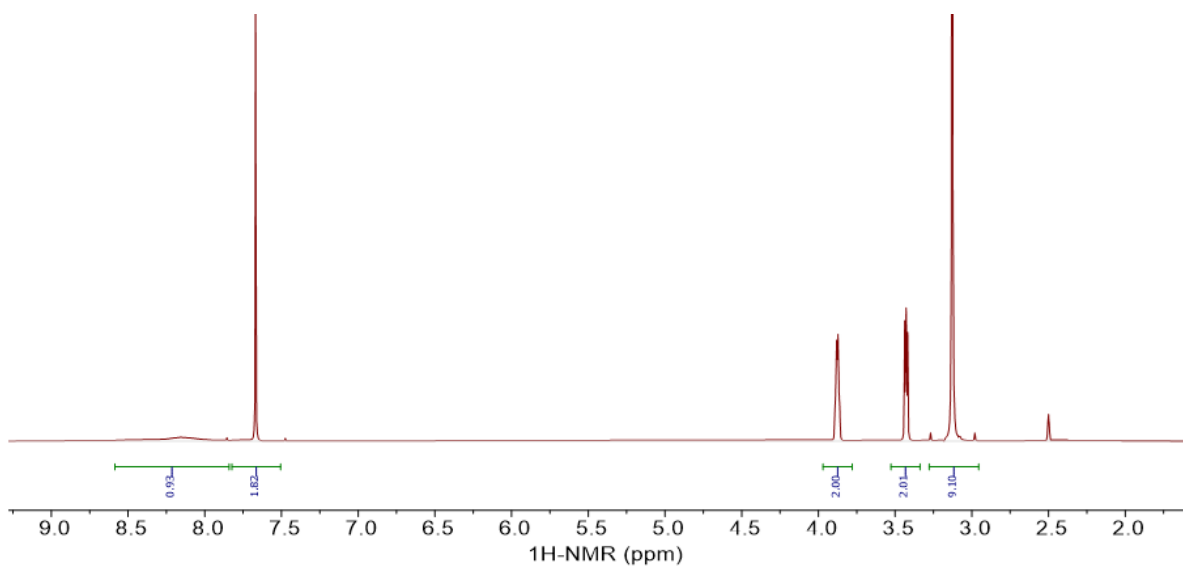


**Figure S19.** Full (a)  $^1\text{H-NMR}$  and (b)  $^{13}\text{C-NMR}$  of  $[\text{Ch}]^+[\text{Cl}]^-$ .

(a)



(b)

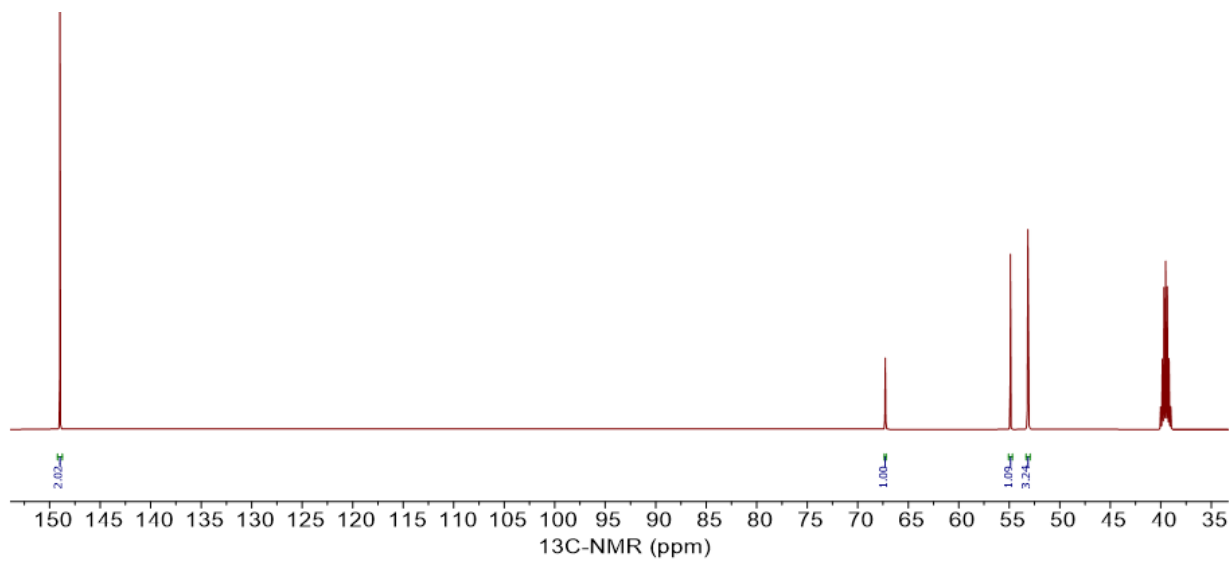
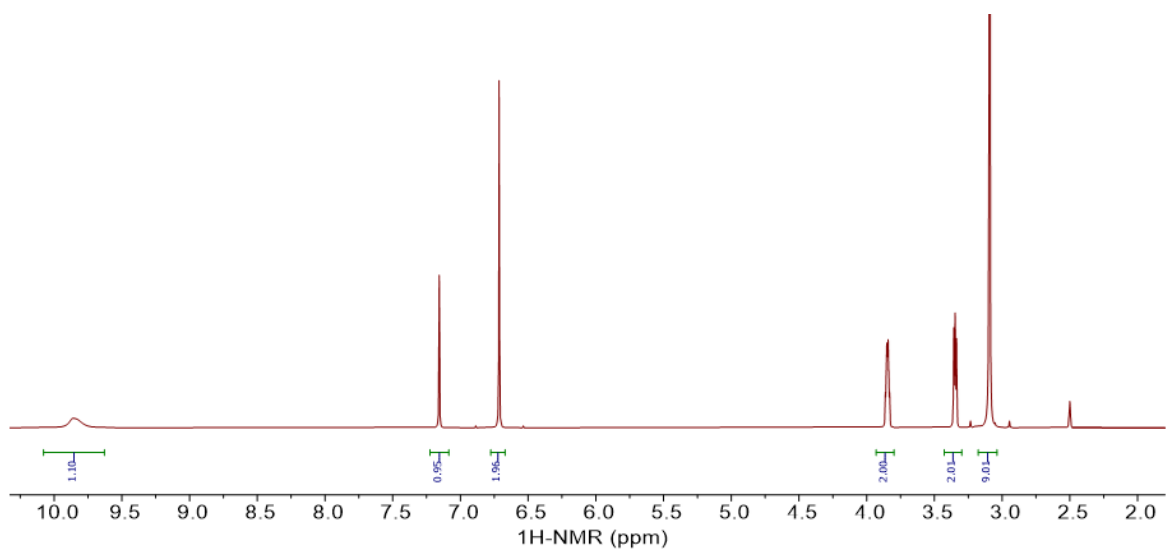


**Figure S20.** Full (a) <sup>1</sup>H-NMR and (b) <sup>13</sup>C-NMR of [Ch]<sup>+</sup>[Trz]<sup>-</sup>.

(a)



(b)

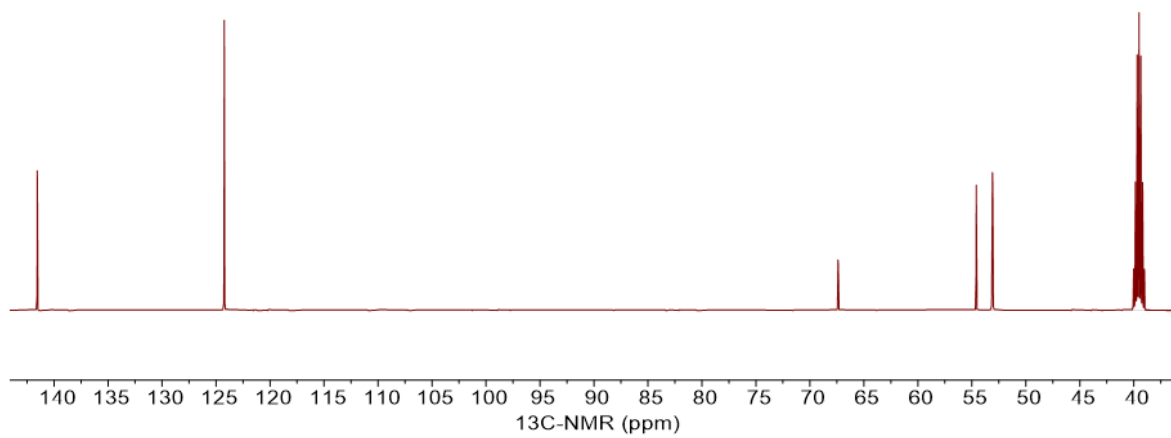
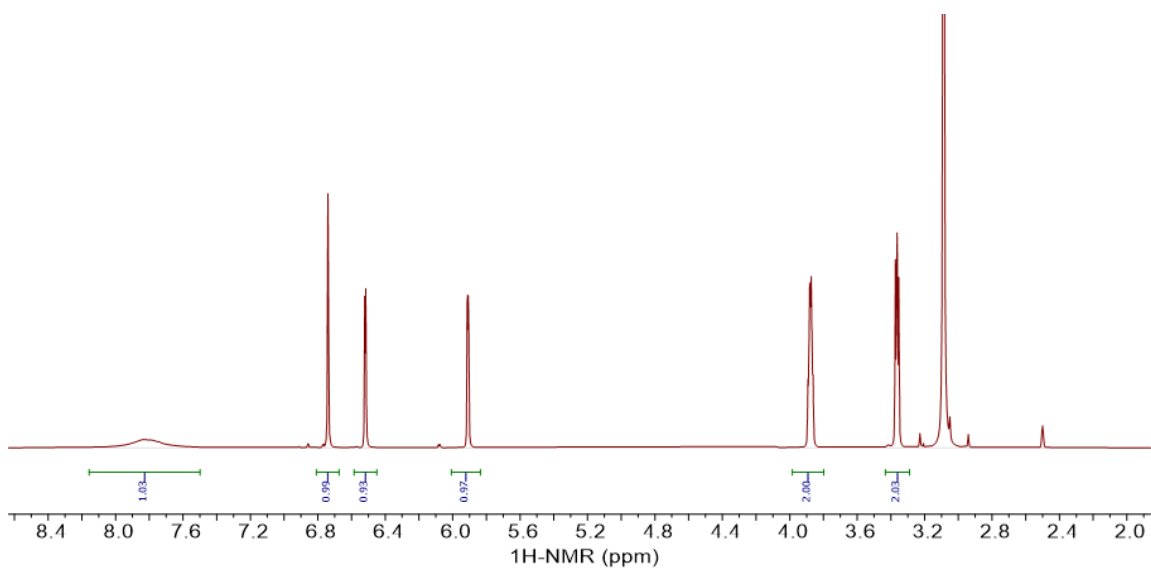


**Figure S21.** Full (a) <sup>1</sup>H-NMR and (b) <sup>13</sup>C-NMR of Ch<sup>+</sup>ImH.

(a)



(b)

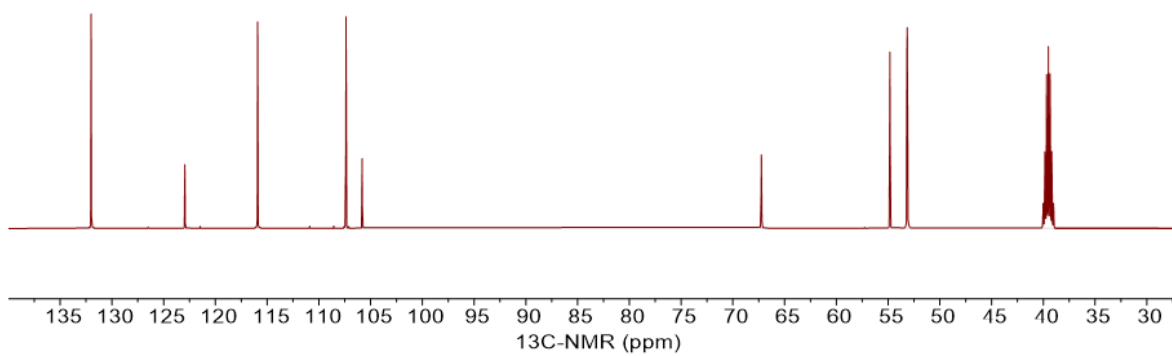
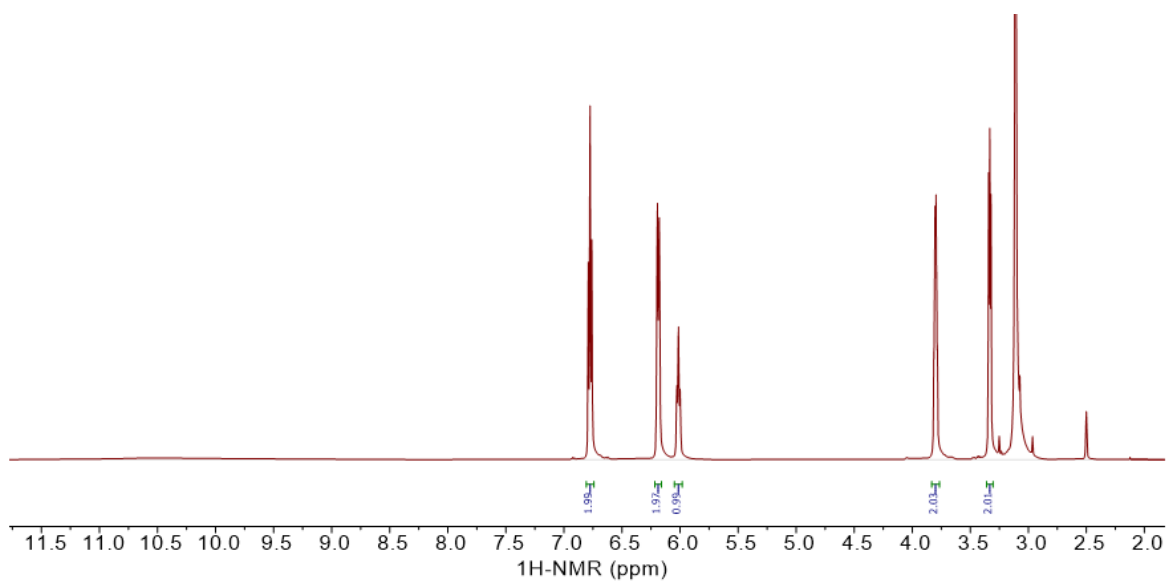


**Figure S22.** Full (a)  $^1\text{H-NMR}$  and (b)  $^{13}\text{C-NMR}$  of  $[\text{Ch}]^+[\text{CNpyr}]^-$ .

(a)



(b)

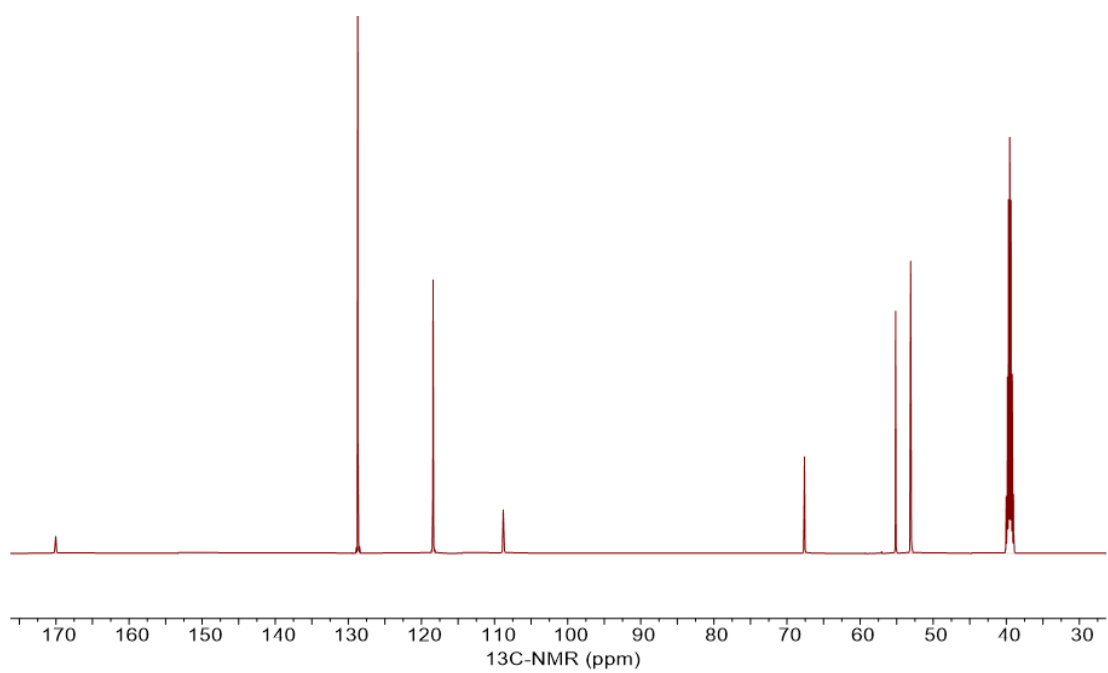


**Figure S23.** Full (a) <sup>1</sup>H-NMR and (b) <sup>13</sup>C-NMR of Ch<sup>±</sup>PhOH.

## REFERENCES

- (1) Lee, Y. Y.; Penley, D.; Klemm, A.; Dean, W.; Gurkan, B. Deep Eutectic Solvent Formed by Imidazolium Cyanopyrrolide and Ethylene Glycol for Reactive CO<sub>2</sub> Separations. *ACS Sustain. Chem. Eng.* **2021**, *9* (3), 1090–1098. <https://doi.org/10.1021/acssuschemeng.0c07217>.
- (2) Lee, Y.; Cagli, E.; Klemm, A.; Park, Y.; Dikki, R. Microwave Regeneration and Thermal and Oxidative Stability of Imidazolium Cyanopyrrolide Ionic Liquid for Direct Air Capture of Carbon Dioxide. *ChemSusChem* **2023**, No. e202300118. <https://doi.org/10.1002/cssc.202300118>.
- (3) G16\_C01 (1). <https://gaussian.com/citation/>.
- (4) Lee, C.; Yang, W.; Parr, R. Development of the Colle-Salvetti Correlation-Energy Formula into a Functional of the Electron Density. *Phys. Rev. B* **1988**, *37* (2), 785.
- (5) Ditchfield, R.; Hehre, W.; Pople, J. Self-consistent Molecular-orbital Methods. IX. An Extended Gaussian-type Basis for Molecular-orbital Studies of Organic Molecules. *J. Chem. Phys.* **1971**, *54* (2), 724–728.
- (6) Wang, C.; Luo, X.; Luo, H.; Jiang, D. E.; Li, H.; Dai, S. Tuning the Basicity of Ionic Liquids for Equimolar CO<sub>2</sub> Capture. *Angew. Chemie - Int. Ed.* **2011**, *50* (21), 4918–4922. <https://doi.org/10.1002/anie.201008151>.
- (7) Li, S.; Zhou, Z.; Zhang, Y.; Liu, M.; Li, W. 1H-1,2,4-Triazole: An Effective Solvent for Proton-Conducting Electrolytes. *Chem. Mater.* **2005**, *17* (24), 5884–5886. <https://doi.org/10.1021/cm0515092>.
- (8) Bordwell, F. G. Equilibrium Acidities in Dimethyl Sulfoxide Solution. *Acc. Chem. Res.* **1988**, *21* (12), 456–463. <https://doi.org/10.1021/ar00156a004>.
- (9) Bunton, C. A.; Diaz, S. Aromatic Nucleophilic Substitution in Nucleophilic Surfactants. Comparison with Alkoxide Reactions. *J. Am. Chem. Soc.* **1976**, *98* (18), 5663–5671. <https://doi.org/10.1021/ja00434a043>.
- (10) Ryu, I. S.; Liu, X.; Jin, Y.; Sun, J.; Lee, Y. J. Stoichiometric Analysis of Competing Intermolecular Hydrogen Bonds Using Infrared Spectroscopy. *RSC Adv.* **2018**, *8* (42), 23481–23488. <https://doi.org/10.1039/c8ra02919a>.
- (11) Wang, Z.; Wu, C.; Wang, Z.; Zhang, S.; Yang, D. CO<sub>2</sub> Capture by 1,2,3-Triazole-Based Deep Eutectic Solvents: The Unexpected Role of Hydrogen Bonds. *Chem. Commun.* **2022**, *58* (53), 7376–7379. <https://doi.org/10.1039/d2cc02503e>.
- (12) Cui, G.; Lv, M.; Yang, D. Efficient CO<sub>2</sub> Absorption by Azolide-Based Deep Eutectic Solvents. *Chem. Commun.* **2019**, *55*, 1426–1429. <https://doi.org/10.1039/c8cc10085c>.
- (13) Sze, L. L.; Pandey, S.; Ravula, S.; Pandey, S.; Zhao, H.; Baker, G. A.; Baker, S. N. Ternary Deep Eutectic Solvents Tasked for Carbon Dioxide Capture. *ACS Sustain. Chem. Eng.* **2014**, No. 2, 2117–2123.
- (14) Klemm, A.; Vicchio, S. P.; Bhattacharjee, S.; Cagli, E.; Park, Y.; Zeeshan, M.; Dikki, R.; Liu, H.; Kidder, M. K.; Getman, R. B.; Gurkan, B. Impact of Hydrogen Bonds on CO<sub>2</sub> Binding in Eutectic Solvents: An Experimental and Computational Study toward Sorbent Design for CO<sub>2</sub> Capture. *ACS Sustain. Chem. Eng.* **2022**, *11*, 3740–3749. <https://doi.org/10.1021/acssuschemeng.2c06767>.